Environmental Science and Pollution Research
https://doi.org/10.1007/s11356-020-09484-8

RESEARCH ARTICLE

Spatiotemporal variation and determinants of population's $PM_{2.5}$ exposure risk in China, 1998–2017: a case study of the Beijing-Tianjin-Hebei region

Ning Jin[1] · Junming Li[2] · Meijun Jin[3] · Xiaoyan Zhang[4]

Received: 5 February 2020 / Accepted: 27 May 2020

Abstract

$PM_{2.5}$ pollution has emerged as a global human health risk. The best measure of its impact is a population's $PM_{2.5}$ exposure ($PPM_{2.5}E$), an index that simultaneously considers $PM_{2.5}$ concentrations and population spatial density. The spatiotemporal variation of $PPM_{2.5}E$ over the Beijing-Tianjin-Hebei (BTH) region, which is the national capital region of China, was investigated using a Bayesian space-time model, and the influence patterns of the anthropic and geographical factors were identified using the GeoDetector model and Pearson correlation analysis. The spatial pattern of $PPM_{2.5}E$ maintained a stable structure over the BTH region's distinct terrain, which has been described as "high in the northwest, low in the southeast". The spatial difference of $PPM_{2.5}E$ intensified annually. An overall increase of 6.192 (95% CI 6.186, 6.203) $\times 10^3$ μg/m^3 · persons/km^2 per year occurred over the BTH region from 1998 to 2017. The evolution of $PPM_{2.5}E$ in the region can be described as "high value, high increase" and "low value, low increase", since human activities related to gross domestic product (GDP) and energy consumption (EC) were the main factors in its occurrence. GDP had the strongest explanatory power of 76% ($P < 0.01$), followed by EC and elevation (EL), which accounted for 61% ($P < 0.01$) and 40% ($P < 0.01$), respectively. There were four factors, proportion of secondary industry (PSI), normalized differential vegetation index (NDVI), relief amplitude (RA), and EL, associated negatively with $PPM_{2.5}E$ and four factors, GDP, EC, annual precipitation (AP), and annual average temperature (AAT), associated positively with $PPM_{2.5}E$. Remarkably, the interaction of GDP and NDVI, which was 90%, had the greatest explanatory power for $PPM_{2.5}E$ ′ s diffusion and impact on the BTH region.

Keywords $PM_{2.5}$ pollution · Population health exposure · Bayesian statistics · Influence factors

Introduction

$PM_{2.5}$ pollution has emerged as a global human health risk (Cohen et al. 2017; Heft-Neal et al. (2018); Lelieveld et al. 2015). $PM_{2.5}$ concentrations constantly serve as a risk indicator for a population's exposure to air pollution (Hystad et al. 2011; Zhong et al. 2013). However, this measure does not take into account the heterogeneity of a population's density. To solve this problem, Kousa et al. (2002) created a revised measure to represent the population's health risk due

Responsible editor: Lotfi Aleya

Ning Jin and Junming Li are Joint first authors with equal contributions

✉ Junming Li
Lijm@sxufe.edu.cn

✉ Meijun Jin
Jinmeijun@tyut.edu.cn

Ning Jin
Jinscut@163.com

Xiaoyan Zhang
Zhangxy@sxufe.edu.cn

[1] School of Mathematics, South China University of Technology, 381 Wushan Road, Guangzhou 510000, China

[2] School of Statistics, Shanxi University of Finance and Economics, 696 Wucheng Road, Taiyuan 030006, China

[3] College of Architecture, Taiyuan University of Technology, 79 Yingze Street, Taiyuan 030024, China

[4] National Academy of Economic Strategy, Chinese Academy of Social Sciences, 28 Shuguanxili Chaoyang District, Beijing 100028, China

Published online: 05 June 2020

to $PM_{2.5}$ exposure: a population's $PM_{2.5}$ exposure ($PPM_{2.5}E$), calculated by multiplying $PM_{2.5}$ concentrations with population density.

As a major metropolitan area of China, the Beijing-Tianjin-Hebei (BTH) region has played an important role in Chinese society and economy, containing about 10% of the total population and about 9% of the gross domestic product (GDP) of China. As a consequence of its population density and activity, the air pollution in the BTH region has created a crucial environmental problem (Yan et al. 2018) and makes BTH the most $PM_{2.5}$-polluted area in China (Wang et al. 2014). Coupled with the high population density in its urban areas, especially in Beijing and Tianjin, the $PM_{2.5}$ problem is gravely serious, yet few researchers have studied the spatiotemporal trends, determinants, or impact factors of $PPM_{2.5}E$, even though some studies have focused on $PM_{2.5}$ concentrations over the BTH region.

Within the existing literature, Yan et al. (2018) used spatial clustering analysis based on Moran's index to explore the space-time evolution of $PM_{2.5}$ concentrations over the BTH region. Huang et al. (2018) studied the critical factors on $PM_{2.5}$ concentrations in the BTH region. Zhao et al. (2020) employed a random forest model to estimate the daily $PM_{2.5}$ concentration with a $0.01° \times 0.01°$ spatial resolution over the BTH region. Shen and Yao (2017) roughly analysed the spatial pattern of $PM_{2.5}$ concentrations and $PPM_{2.5}E$ in the four urban agglomerations of China in 2014, and calculated the Pearson correlation coefficient (PCC) between GDP and $PM_{2.5}$ concentrations, $PPM_{2.5}E$, respectively. Wang et al. (2019) and Ni et al. (2018) also explored the spatiotemporal variation of $PM_{2.5}$ concentrations in the BTH region.

However, given the advantages of the $PPM_{2.5}E$ index and limited research on spatiotemporal trends and determinants of $PPM_{2.5}E$ in the BTH region, our study employed a Bayesian spatiotemporal model and GeoDetector model to investigate the space-time evolution and determinants of $PPM_{2.5}E$ in the BTH region, based on remotely sensed data of $PM_{2.5}$ concentrations, population density, and 2015 yearbook statistics data at the county level.

Methods

Study area

The Beijing-Tianjin-Hebei (BTH) region was chosen as the study area for several reasons. Beijing and Tianjin are international megalopolises that serve as the political and economic centre of China. This area is located in North China (Fig. 1), between 36° 42′–40° 08′ N and 114° 54′–117° 46′ E, and covers a land area of about 218 thousands km^2 with approximately 1.1 hundred million inhabitants (China, the data of the Sixth Population Census, 2010). As a consequence of this size, population density, and importance, the BTH region faces the most severe environmental problems in China and has been targeted to be developed into an "environmental improvement demonstration region" (Chen et al. 2018; Gao et al. 2014).

Materials

The first dataset used in this research included remotely sensed annual average $PM_{2.5}$ concentrations with a spatial resolution of $0.1° \times 0.1°$ (~ 10 km × 10 km). The remotely sensed $PM_{2.5}$ data products were produced in three steps by van Donkelaar's team (van Donkelaar et al. 2015, 2016). Firstly, the aerosol optical depth (AOD) data were retrieved from multiple satellite products, the MODerate resolution Imaging Spectroradiometer (MODIS), the Multiangle Imaging SpectroRadiometer (MISR), and the Sea-viewing Wide Field-of-view Sensor (SeaWiFS). Secondly, the GEOS-Chem chemical transport model (http://geos-chem.org) was used to simulate the spatiotemporally varying geophysical relationship between AOD and $PM_{2.5}$ concentrations based on their relative uncertainties determined by the ground-based sun photometer (AERONET) observations. And then the multiple retrieved AOD data were combined with the GEOS-Chem simulations. Thirdly, the bias in the annual mean of these geophysically based satellite $PM_{2.5}$ was predicted by the geographically weighted regression (GWR) model. The details and validation of the dataset can be found in the related references (van Donkelaar et al. 2015, 2016).

The second dataset included a global population density data whose spatial resolution was $2.5' \times 2.5'$ (~5 km × 5 km) in 2000, 2005, 2010, and 2015 (Center for International Earth Science Information Network - CIESIN - Columbia University 2017). This population density dataset was consistent with national censuses and population registers as rasterized data to facilitate data integration. The continuous yearly population density data of the BTH region from 1998 to 2017 were obtained by the linear interpolation method (van Donkelaar et al. 2015). The spatial resolutions and projected coordinate system of remotely sensed annual $PM_{2.5}$ concentrations were adjusted in accordance with the population density dataset with a spatial resolution of ($2.5' \times 2.5'$, ~5 km × 5 km) while the BTH region's $PPM_{2.5}E$ was calculated through multiplying the $PM_{2.5}$ concentrations by the population density in the same spatial lattice unit.

The third datasets were the influencing factors, which included two categories of data: human activities and natural environmental factors. The former included three covariates: gross domestic product (GDP), proportion of the secondary industry (PSI), and energy consumption (EC). EC was represented with nightlight remote sensing data. GDP and PSI were collected from the provincial statistical yearbook of the BTH region in the corresponding year.

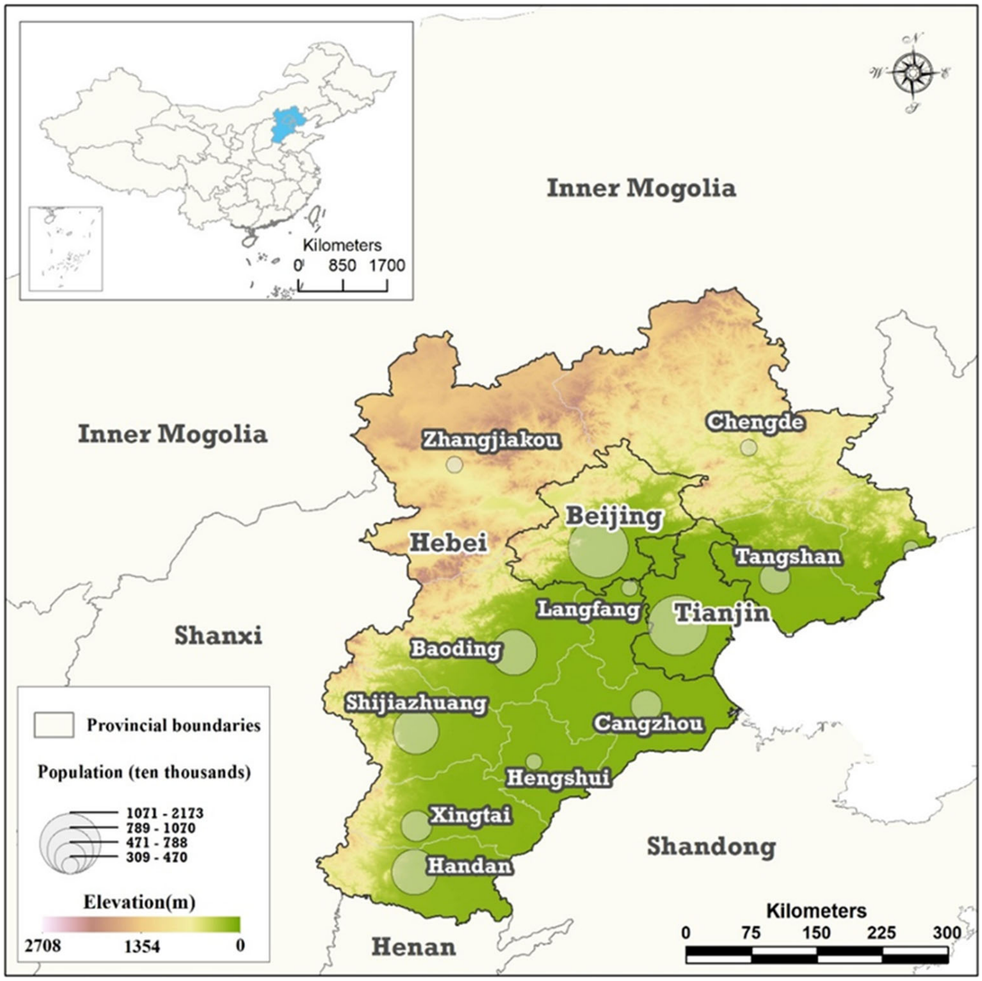

Fig. 1 Geographical location of the study area

The yearbook contained six covariates: annual precipitation (AP), annual average temperature (AAT), normalized differential vegetation index (NDVI), relief amplitude (RA), annual relative humidity (ARH), and elevation (EL). The meteorological data (AP, AAT, and ARH) were downloaded from the Website of China (http://data.cma.cn/site/index.html). RA was calculated with the standard deviation of elevation divided by the mean value of elevation in the BTH region. The lattice data of the elevation and NDVI in the BTH region were downloaded from the Resource and Environment Data Cloud Platform (http://www.resdc.cn).

Bayesian space-time model

A Bayesian space-time model (BSTM) (Li et al. 2014) was employed in our study to investigate the spatiotemporal patterns of $PPM_{2.5}E$ in the BTH region from 1998 to 2017. The BSTM, which integrates the Bayesian hierarchical model and spatiotemporal interaction model, can decompose the intricate space-time process to three components: overall spatial trend, overall temporal trend, and local trend (Bernardinelli et al. 1995; Li et al. 2014). The $PPM_{2.5}E$ can be calculated as follows (Peng et al. 2016):

$$R_{it} = \Theta_{it} * \Omega_{\mathrm{it}} \tag{1}$$

R_{it} represents the $PPM_{2.5}E$ value ($\times 10^3 \mu g/m^3 \cdot$ persons/km^2) in the ith spatial unit in the tth year. Θ_{it} and Ω_{it} are annual $PM_{2.5}$ concentrations and population density in the ith spatial unit in the tth year. Considering that $PPM_{2.5}E$ is a continuous variable, the likely distribution of the observed $PPM_{2.5}E$ was assigned in this way:

$$y_{it} \sim \mathrm{Normal}\left(\eta_{it}, \sigma_y^2\right) \mathrm{I}(0,) \forall \mathrm{PPM}_{2.5}\mathrm{E} \text{ observed data} \tag{2}$$

where y_{it} represents the observed $PPM_{2.5}E$ of the ith provincial area in the tth year, η_{it} represents the corresponding mean values, σ_y^2 is the corresponding variances of y_{it}, and I(0,) denotes the range of greater than zero. The space-time process model of $PPM_{2.5}E$ in the BTH region from 1998 to 2017 can be expressed with the following:

$$\eta_{it} = \gamma + S_i + (K_0 t + v_t) + k_i t + \epsilon_{it} \tag{3}$$

$\forall i \in$ spatial domain $\forall t \in$ time domain: 1998–2017

$$\gamma \sim Uniform(-\infty, +\infty) \quad (4)$$

$$S_i \sim CAR.Normal\left(adj.S_{y_i}, adj.S_{n_i}, adj.W_i, \tau_s^2\right) \quad (5)$$

$$k_i \sim CAR.Normal\left(adj.S_{y_i}, adj.S_{n_i}, adj.W_i, \tau_k^2\right) \quad (6)$$

$$\epsilon_{it} \sim \text{iid } Normal\left(0, \sigma_\epsilon^2\right) \quad (7)$$

where γ, whose priors used non-informative prior distribution, represents the basic level of $PPM_{2.5}E$ over the BTH region from 1998 to 2017, S_i represents the common spatial relative magnitude of the $PPM_{2.5}E$ in the ith spatial unit, and $(K_0 t + v_t)$ describes the overall trend of the $PPM_{2.5}E$ over the BTH region from 2013 to 2017. The parameter v_t describes the non-linear variation of the overall trend, and its prior was assigned with Gauss distribution. The prior distributions of the parameter of the overall spatial relative magnitude and the local trend, S_i, k_i, were assigned using the Besag York Mollie (BYM) model (Besag et al. 1991) and integrated using a conditional autoregressive (CAR) normal prior describing the spatial structured and unstructured effects, denoted by *CAR. Normal*(.) in formulas (5) and (6). The terms $adj.S_{y_i}$, $adj.S_{n_i}$, and $adj.\ W_i$ stand for the spatial adjacency units, numbers, and weights, respectively. The spatial adjacency relationship adopts the first-order "Queen" adjoining form. The term ϵ_{it} represents the Gaussian random effects, whose prior distributions were assigned with normal distributions. The prior distributions of the reciprocals of all variances (i.e. $1/\sigma_y^2$ and $1/\tau_s^2$, $1/\tau_k^2$ and $1/\sigma_\epsilon^2$) were assigned with Gamma distribution.

Bayesian inferences in this research were conducted in WinBUGS 1.4 (Lunn et al. 2000). All parameters' posterior distributions of the model were estimated by Markov chain Monte Carlo (MCMC) simulations. The convergence of Bayesian inferences was evaluated by the Gelman-Rubin statistical coefficient (Gelman and Rubin 1992); the closer the coefficient is to 1.0, the better the convergence is. The Gelman-Rubin coefficients were less than 1.03 for all parameters.

GeoDetector model

The GeoDetector model was first presented by Wang et al. (2010) in 2010. The q-statistic value estimated from the GeoDetector model can measure the degree of spatial stratified heterogeneity (Wang et al. 2016). The idea behind the GeoDetector model is that two variables would be (linearly or non-linearly) coupled in strata if one causes another or if there is association with each other. The difference between the GeoDetector model and the ordinary linear regression model is that the former will not only investigate the non-linear association but also the interaction effects between various variables (Yang et al. 2018). The magnitude of the q-statistic value can quantify the influencing power of the single factor or interaction among the different factors. The q-statistic value, q, can be calculated by the following formula (8):

$$q = 1 - \frac{\sum_{h=1}^{L} \sum_{i=1}^{N_h} \left(Y_{hi} - \overline{Y}_h\right)^2}{\sum_{i=1}^{N} \left(Y_i - \overline{Y}\right)^2} \times 100\%$$

$$= 1 - \frac{\sum_{h=1}^{l} N_h \sigma_h^2}{N\sigma^2} \times 100\% \quad (8)$$

where N is the number of the spatial lattice pixels over the BTH region stratified into the $h = 1, 2, \ldots, L$ stratum according to influencing factors, Xs; stratum h includes N_h spatial statistical pixels; and Y_i and Y_{hi} denote the $PPM_{2.5}E$ of the ith pixel and in stratum h of the influencing factors, Xs, separately. $\overline{Y}$ and σ^2 represent the common mean and variance of $PPM_{2.5}E$ over the BTH region. The stratum mean and variance, $\overline{Y}_h$ and σ_h^2, can be expressed as follows:

$$\overline{Y}_h = \frac{\sum_{i=1}^{N_h} Y_{hi}}{N_h}, \quad \sigma_h^2 = \frac{\sum_{i=1}^{N_h} \left(Y_{hi} - \overline{Y}_h\right)^2}{N_h} \quad (9)$$

where the q-statistic value is between 0 and 100%. The larger the q-statistic value is, the stronger the influence of variable X on Y.

The q-statistic value was calculated based on the cross-classified stratum of two different factors: $X1$ and $X2$, $q(X1 \cap X2)$. This value can identify the interaction effects of $X1$ and $X2$ on the dependent variable, Y. The GeoDetector model provides the judging rules to assess the types of effects the interaction of $X1$ and $X2$ have on Y (Table 1) (Wang and Hu 2012; Wang et al. 2010; Yang et al. 2018). The model can

Table 1 The interactive categories of two factors and the interactive relationship

Judging rules	Types of the interaction effects
$q(X1 \cap X2) < Min\,(q(X1), q(X2))$	Non-linearly weakened
$Min(q(X1), q(X2)) < q(X1 \cap X2) < Max\,(q(X1), q(X2))$	Univariate non-linearly weakened
$q(X1 \cap X2) > Max\,(q(X1), q(X2))$	Bivariate enhanced
$q(X1 \cap X2) = q(X1) + q(X2)$	Independent
$q(X1 \cap X2) > q(X1) + q(X2)$	Non-linearly enhanced

also identify whether the two factors, $X1$ and $X2$, weaken or enhance the influence on Y. The interaction effects can be explained as five types of interactive relationships. Specifically, the interaction effect can be identified as non-linearly weakened if the interaction q-statistic value, denoted as $q(X1 \cap X2)$, is less than the minimum of $q(X1)$ and $q(X2)$; as univariate non-linearly weakened if $q(X1 \cap X2)$ is between the minimum and maximum of $q(X1)$ and $q(X2)$; as bivariate enhanced if $q(X1 \cap X2)$ is greater than the maximum of $q(X1)$ and $q(X2)$; as independent if $q(X1 \cap X2)$ is equal to the sum of $q(X1)$ and $q(X2)$, $q(X1) + q(X2)$; and as non-linearly enhanced if $q(X1 \cap X2)$ is greater than $q(X1) + q(X2)$.

Results

Descriptive statistics of spatial $PPM_{2.5}E$ distribution

Generally, the spatial pattern of $PPM_{2.5}E$ maintained a stable structure from 2000 to 2015. However, an increase occurred in several cities, including Beijing, Tianjin, and Shijiazhuang. Figure 2 shows the geospatial distribution of $PPM_{2.5}E$ in the BTH region in 2000, 2005, 2010, and 2015. Five cities (Beijing, Tianjin, Baoding, Shijiazhuang, and Handan) experienced $PPM_{2.5}E$ with greater than 1000×10^3 $\mu g/m^3 \cdot persons/km^2$ in 2000, and $PPM_{2.5}E$ in Tangshan and Xingtai also exceeded 1000×10^3 $\mu g/m^3 \cdot$ persons/km^2. In addition, the mean and maximum of $PPM_{2.5}E$ increased from 23.37×10^3 and 1643.79×10^3 in 2000 to 42.02×10^3 and 2744.95×10^3 $\mu g/m^3 \cdot$ persons/km^2 in 2015. Likewise, the spatial heterogeneity of $PPM_{2.5}E$ over the BTH region increased from 2000 to 2015, and the coefficient of variation (CV) increased from 2.90 in 2000 to 3.32 in 2015.

Spatiotemporal trends

Overall spatial trends

Figure 3 illustrates the estimated common spatial relative magnitude. This calculation involves the posterior median of the parameter, $\exp(S_i)$, which directly quantifies the $PPM_{2.5}E$ magnitude in the ith spatial pixel relative to the average level

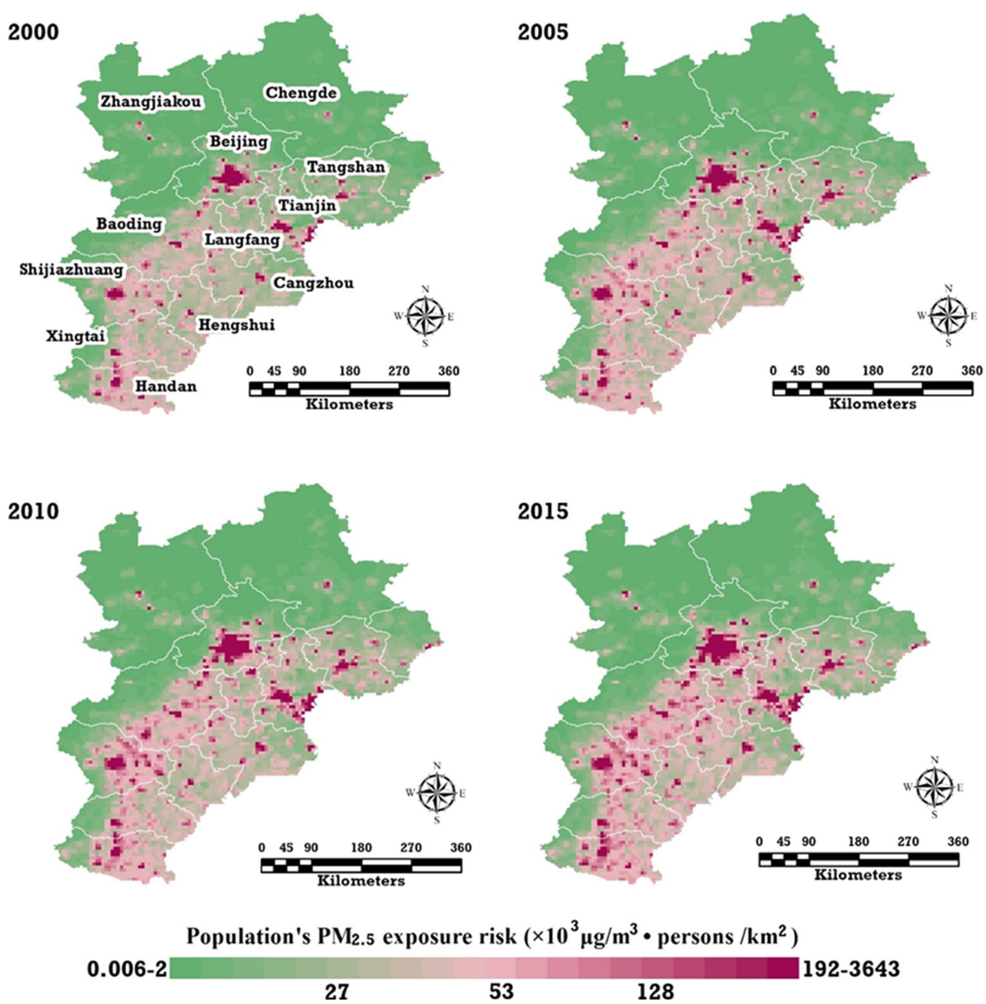

Fig. 2 Geospatial distribution of $PPM_{2.5}E$ in the Beijing-Tianjin-Hebei area in 2000, 2010, and 2015

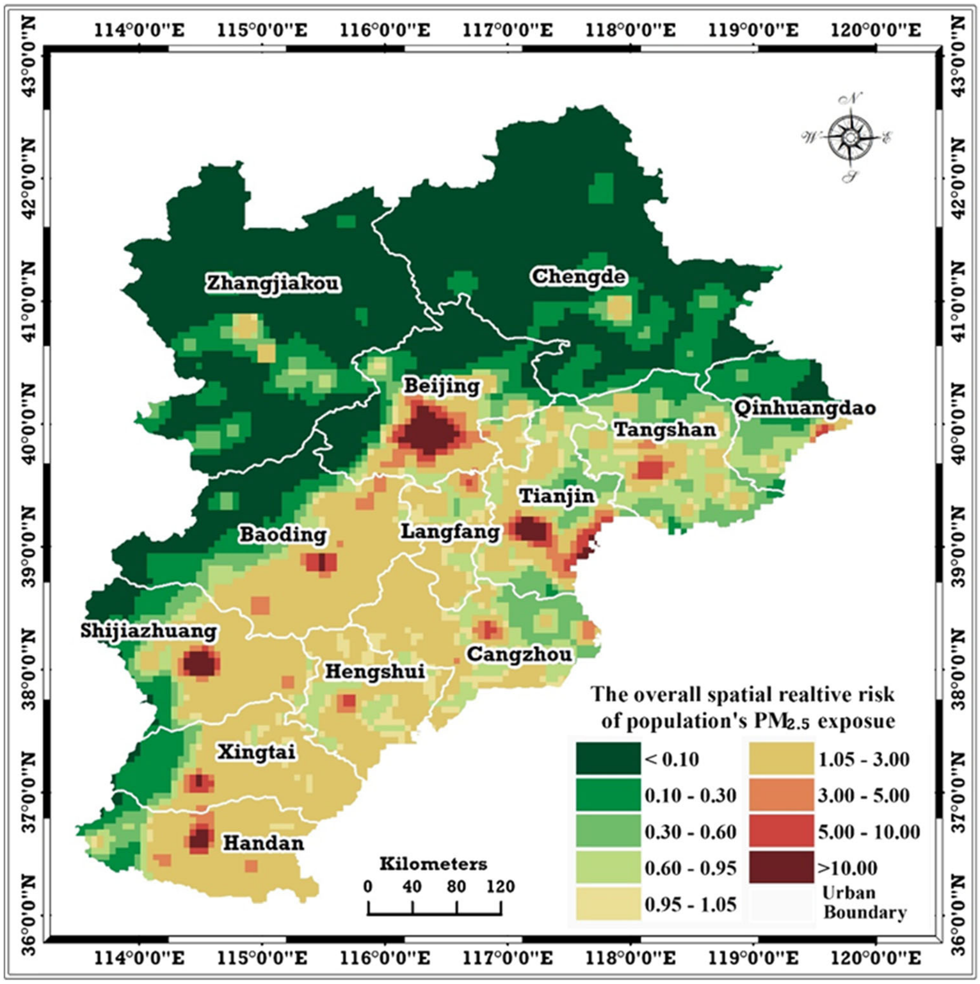

Fig. 3 The common spatial relative magnitude of $PPM_{2.5}E$ over the BTH region, including the posterior medians of the parameter, $\exp(S_i)$, estimated from the BSTM

over the BTH region, namely the $PPM_{2.5}E$ of the ith spatial pixel, times the average level over the BTH region. Generally, the common spatial pattern of the level of $PPM_{2.5}E$ over the BTH region exhibited a distinct geographical feature, described as "high in the northwest, low in the southeast". Beijing is the largest area in the region with a common spatial relative magnitude of $PPM_{2.5}E$ that is greater than 5.0. The northern two cities, Chengde and Zhangjiakou, have the lowest level of $PPM_{2.5}E$ among all 13 cities. Their corresponding common spatial relative magnitudes are all less than 3.0. In addition, the maximums of the common spatial relative magnitude of $PPM_{2.5}E$ in Beijing, Tianjin, and Shijiazhuang are 47.27 (45.40, 49.12), 29.79 (22.28, 37.45), and 31.35 (24.53, 38.24), respectively.

Overall and local trends

The overall trend, K_0, estimated by the BSTM was 6.192 (95% CI 6.186, 6.203) $\times 10^3$ $\mu g/m^3 \cdot$ persons/km^2 per year. The local trends of $PPM_{2.5}E$ in each pixel over the BTH region, k_i, were estimated by the BSTM. Figure 4 shows the local trends of $PPM_{2.5}E$ over the BTH region from 1998 to 2017, including the posterior medians of the parameter, k_i ($\times 10^3$ $\mu g/m^3 \cdot$ persons/km^2 per year), estimated from the BSTM. The results show that the spatial structure of the local trends is similar to that of the common spatial relative magnitude, namely "high in the northwest, low in the southeast". The highest increase of $PPM_{2.5}E$ occurred in metropolises: specifically, Beijing, Tianjin, Shijiazhuang, Baoding, and Tangshan. Furthermore, local trends greater than 50.0 $\times 10^3$ $\mu g/m^3 \cdot$ persons/km^2 *per year* only occurred in Beijing and Tianjin, and one greater than 53.0 $\times 10^3$ $\mu g/m^3 \cdot$ persons/km^2 per year appeared only in Beijing. Thus, the maximal local trend, 91.76 $\times 10^3$ $\mu g/m^3 \cdot$ persons/km^2 per year, emerged in Beijing. In contrast, the urban areas in Chengde, Zhangjiakou, Hengshui, and Cangzhou experienced a smaller increase in $PPM_{2.5}E$.

Influencing factors

Univariate analysis

This paper investigated the influence factors of $PPM_{2.5}E$ over the BTH region using the GeoDetector model. Two categories

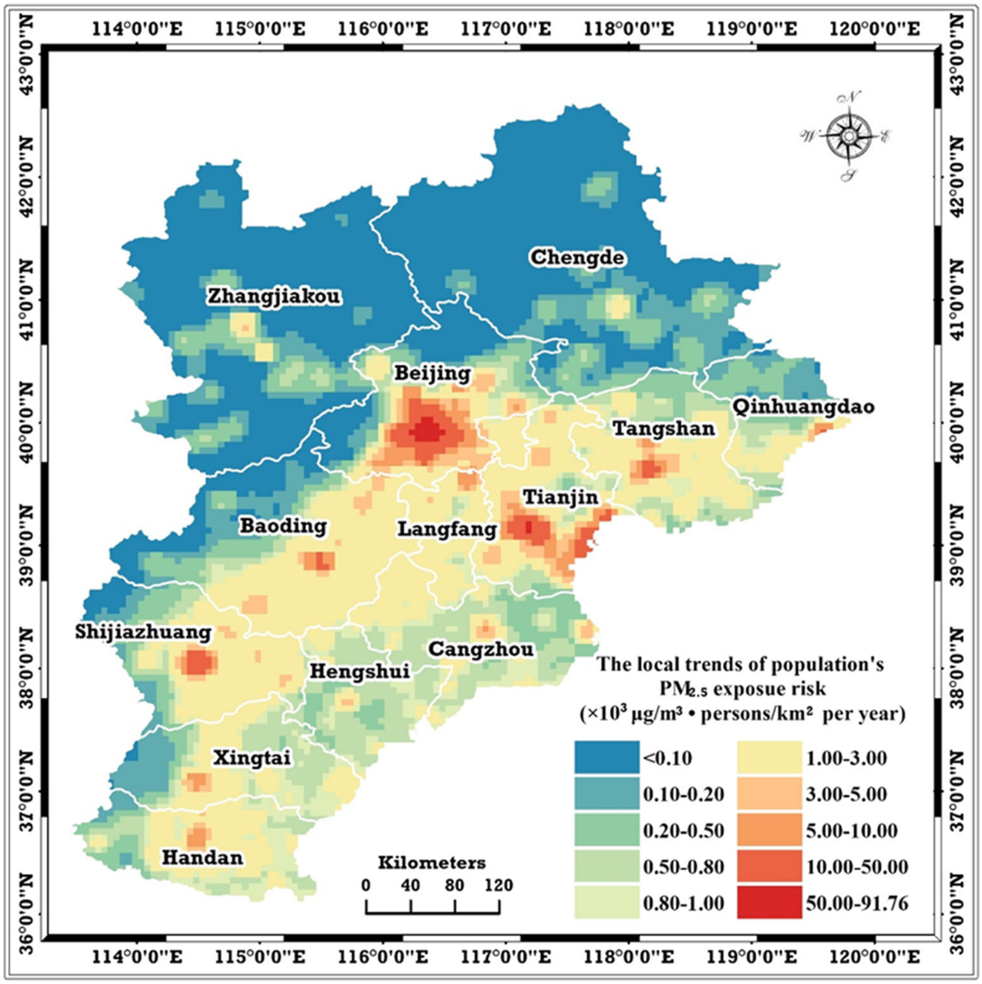

Fig. 4 The local trends of $PPM_{2.5}E$ over the BTH region from 1998 to 2017, including the posterior medians of the parameter, k_i ($\times 10^3$ μg/m^3 · persons/km^2 per year), estimated from the BSTM

of influence factors, human activities and natural environmental factors, and nine proxy variables (Figure 5) were studied. Table 2 lists the results of univariate analysis estimated by the GeoDetector model. In general, the economic factors exerted greater influence than the natural environmental factors. With the exception of PSI, the q-statistic values of GDP and EC

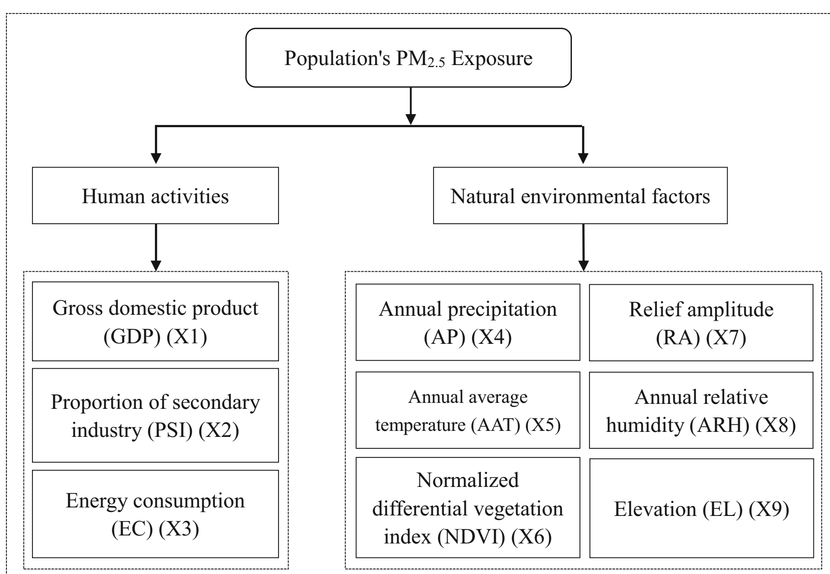

Fig. 5 Diagram of the influencing factors covering the two categories of variables represented by nine proxy variables

Table 2 The results of univariate analysis estimated by the GeoDetector model for influence factors

Factors	Proxy variables	q-statistics values
Economic factors	Gross domestic product (GDP)	0.76 ($P<0.01$)
	Proportion of secondary industry (PSI)	0.19 ($P<0.01$)
	Energy consumption (EC)	0.61 ($P<0.01$)
Natural environmental factors	Annual precipitation (AP)	0.26 ($P<0.01$)
	Annual average temperature (AAT)	0.35 ($P<0.05$)
	Normalized differential vegetation index (NDVI)	0.34 ($P<0.05$)
	Relief amplitude (RA)	0.30 ($P<0.05$)
	Annual relative humidity (ARH)	0.28 ($P<0.01$)
	Elevation (EL)	0.40 ($P<0.05$)

were greater than those of all the natural environmental factors. In particular, among the nine influence factors, GDP had the strongest explanatory power for $PPM_{2.5}E$, with a corresponding q-statistic value of 0.76 ($P<0.01$). EC and EL followed GDP in this regard, with q-statistic values of 0.61 ($P<0.01$) and 0.40 ($P<0.01$), respectively. The bottom three weakest influence factors were PSI, AP, and ARH, whose relevant q-statistic values were 0.19 ($P<0.05$), 0.26 ($P<0.05$), and 0.28 ($P<0.05$), respectively.

To identify the relationship between the nine influencing factors and $PPM_{2.5}E$ over the BTH region, the Pearson correlation coefficients (PCC) between $PPM_{2.5}E$ and the nine factors (Fig. 6) were studied. The PCC of PSI (− 0.15), AP (0.26), and ARH (0.02) were all less than 0.30, indicating that the linear associations between $PPM_{2.5}E$ and the two factors were weak. This result is consistent with that of the GeoDetector model. Moreover, PSI, NDVI, RA, and EL associated negatively with $PPM_{2.5}E$, whereas GDP, EC, AP, and AAT associated positively with $PPM_{2.5}E$. A comparison of the PCC and GeoDetector model results shows that the q-statistics values of the GeoDetector model are greater than the PCCs of the Pearson correlation analysis. However, the

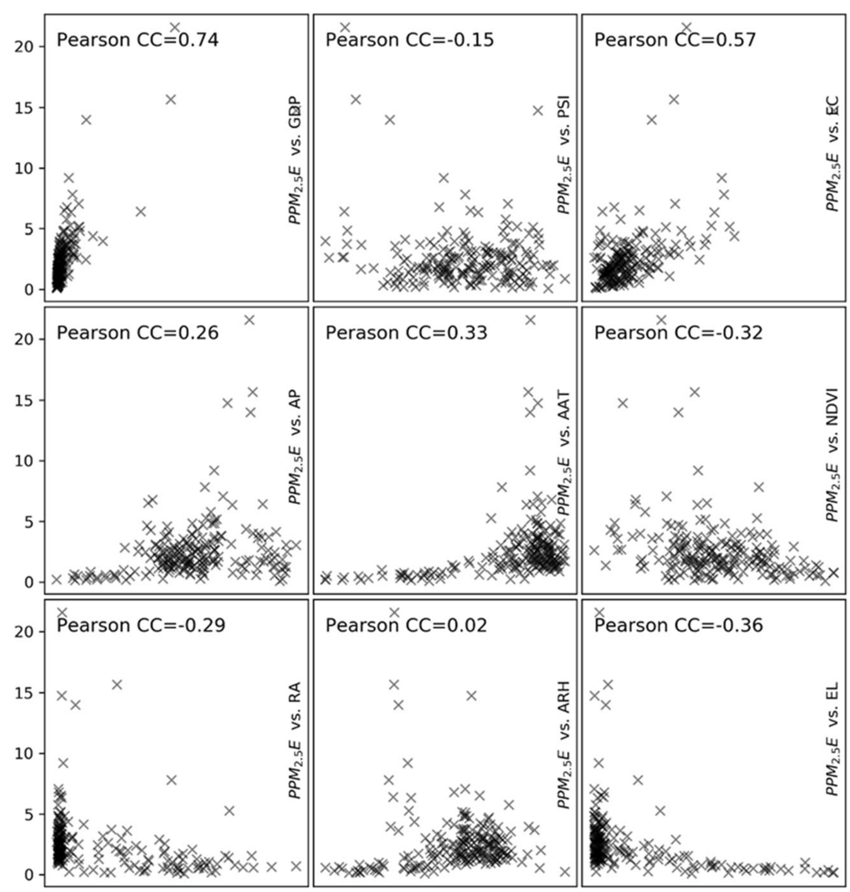

Fig. 6 The Pearson correlation coefficient between $PPM_{2.5}E$ and the nine influencing factors over the BTH region

influencing patterns of the two methods are coherent with each other. Regarding ARH, although the PCC is 0.02, the q-statistic value is 0.28, implying that ARH associates non-linearly with $PPM_{2.5}E$.

The interactive influences of the nine factors

Through univariate analysis, the interactive influences of the nine factors were revealed by the GeoDetector model. The results showed that there were only two types of interaction effects: bivariate enhanced and non-linear enhanced. Figure 7 illustrates the results of the interactive q-statistics values with non-linear enhanced interactive effects from two different factors that were estimated by the GeoDetector model. Figure 8 shows the network diagram of the interactive factors whose interactive q-statistic values were greater than 0.70. The results show that there are seven pairs of two factors with interactive q-statistic values greater than 0.80: GDP and NDVI, PSI and EC, GDP and RA, AP and NDVI, EC and ARH, NDVI and ARH, EC and AAT. In addition, there are seven pairs of two factors with interactive q-statistic values between 0.70 and 0.80. The interaction of GDP and NDVI had the greatest explanatory power, 90.0%, for $PPM_{2.5}E$ over the BTH region.

Figure 8 shows that EC has the greatest number of other factors (PSI, AAT, EL, ARH, AP, and NDVI) with a non-linear enhanced interaction greater than 70.0%. AP, PSI, ARH, and NDVI also interacted with 4 other factors with a non-linear enhanced interaction greater than 70.0%.

Discussion

Our study initially used the BSTM to investigate the spatio-temporal trends of $PPM_{2.5}E$ over the BTH region from 1998 to 2017. Next, the influence factors were explored with the GeoDetector model. Although the spatial pattern of $PPM_{2.5}E$ over the BTH region remained stable, a remarkable increase in $PPM_{2.5}E$ emerged in most regions, especially several big cities, across the BTH region.

$PPM_{2.5}E$ is very different from $PM_{2.5}$ concentrations. The former is determined simultaneously by both $PM_{2.5}$ concentrations and population density. As a result, the levels of $PPM_{2.5}E$ in urban areas of the 13 cities are higher than in the rural areas of the BTH region. In particular, the urban areas of the two megalopolises, Beijing and Tianjin, experienced the highest level of $PPM_{2.5}E$ over the BTH region. Our study found that the spatial structure of the local trends of $PPM_{2.5}E$ is similar to that of the common spatial pattern. In other words, the regions with higher levels of $PPM_{2.5}E$ experienced higher local trends. This phenomenon can be described as "high value, high increase" and "low value, low increase".

The influence patterns of $PPM_{2.5}E$ over the BTH region identified by the GeoDetector model and Pearson correlation analysis indicate that GDP and EC are the main influence factors on $PPM_{2.5}E$. Natural environmental factors also influence $PPM_{2.5}E$, though the corresponding influence magnitudes are not as high. With the exception of GDP and EC, the influence magnitudes of the single factors were otherwise all less than 0.50. The Pearson correlation analysis revealed that PSI associated negatively with $PPM_{2.5}E$ over the BTH region. A previous study (Huang et al. 2018) found secondary industry output correlated positively with $PM_{2.5}$ concentrations over the BTH region. This difference comes from the fact that $PPM_{2.5}E$ is mainly determined by population density and is high in some cities with a high proportion of tertiary industries but low PSI. However, the interactive influencing magnitudes of the two different factors increased remarkably. This phenomenon indicates that the influencing pattern mainly consists of interactive human activities and natural environmental factors.

Despite these results, our study had some limitations. The first is that the spatial resolution of $PPM_{2.5}E$,~5 km × 5 km is not so high. It would be better if the spatial resolution could be 1 km × 1 km or finer. The second is that population density does not consider age structure. It is well-known that the

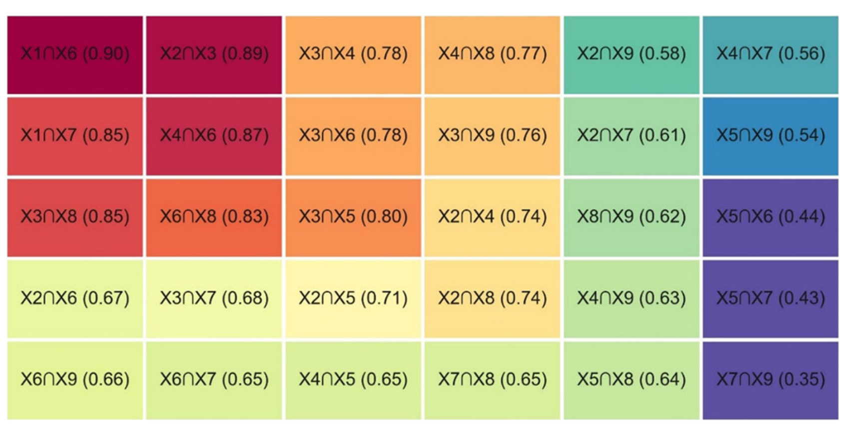

Fig. 7 The results of the interactive q-statistics values with non-linear enhanced interactive effects of two different factors that were estimated by the GeoDetector model

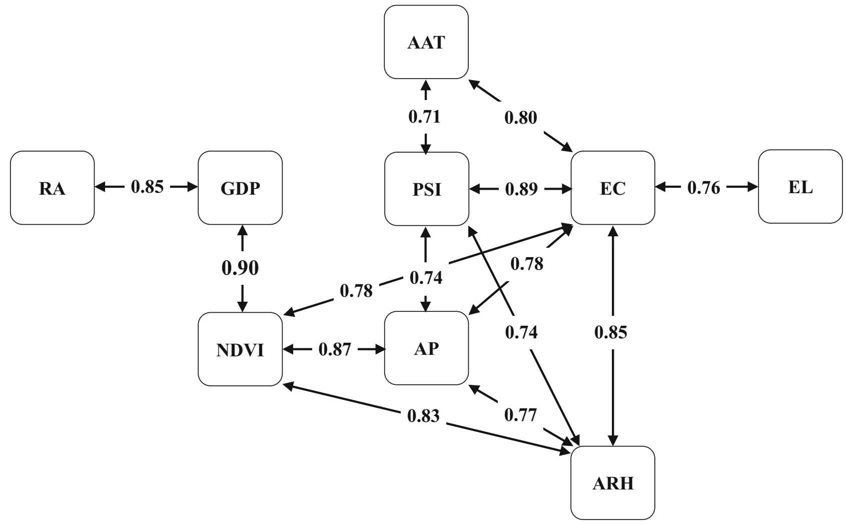

Fig. 8 The network diagram of the interactive factors whose interaction q-statistic values was greater than 0.70

ageing population is more sensitive to $PM_{2.5}$ pollution. Therefore, the ageing population's $PM_{2.5}$ exposure should be researched in future work.

Conclusions

The space-time variation of $PPM_{2.5}E$ over the BTH region from 1998 to 2017 was researched using the BSTM. Then the influence patterns of the nine factors on $PPM_{2.5}E$ in 2015 were investigated using the GeoDetector model and Pearson correlation analysis. This study led to several conclusions.

The common spatial pattern of $PPM_{2.5}E$ over the BTH region maintained a stable structure and exhibited a distinct geographical feature, described as "high in the northwest, low in the southeast". Moreover, the spatial heterogeneity of $PPM_{2.5}E$ over the BTH region increased from 2000 to 2015, and the CV increased from 2.90 in 2000 to 3.32 in 2015. An increase of $PPM_{2.5}E$ with 6.192 (95% CI 6.186, 6.203) $\times 10^3$ $\mu g/m^3 \cdot persons/km^2$ per year occurred over the BTH region from 1998 to 2017. The spatial structure of the local trends is similar to that of the common spatial relative magnitude. This feature of the local trends can be described as "high value, high increase" and "low value, low increase". GDP and EC were the main influence factors on $PPM_{2.5}E$ over the BTH region. GDP had the strongest explanatory power for $PPM_{2.5}E$. The corresponding q-statistic value was 0.76 ($P < 0.01$), followed by EC and EL whose q-statistic values were 0.61 ($P < 0.01$) and 0.40 ($P < 0.01$), respectively. PSI, NDVI, RA, and EL associated negatively with $PPM_{2.5}E$. GDP, EC, AP, and AAT associated positively with $PPM_{2.5}E$. The interactive influencing magnitudes of the two different factors increased remarkably. The interaction of GDP and NDVI had the greatest explanatory power, 90.0%, on $PPM_{2.5}E$ over the BTH region.

Acknowledgements The authors give thanks to Dr. Aaron van Donkelaar of the Atmospheric Physics Institute at Dalhousie University in Canada, who offered the remotely sensed $PM_{2.5}$ data used in this study. Our deepest gratitude is expressed to our anonymous reviewers and editors for their careful work and constructive suggestions that have helped improve our paper substantially.

Funding information This paper is supported by General Project on Humanities and Social Science Research of the Chinese Ministry of Education (19YJCZH079) and China Postdoctoral Fund (2019M650946).

References

Bernardinelli L, Clayton D, Pascutto C, Montomoli C, Ghislandi M, Songini M (1995) Bayesian analysis of space—time variation in disease risk. Stat Med 14:2433–2443

Besag J, York J, Mollié A (1991) Bayesian image restoration, with two applications in spatial statistics. Ann Inst Stat Math 43:1–20

Center for International Earth Science Information Network - CIESIN - Columbia University (2017) Gridded Population of the World, Version 4 (GPWv4): population count, Revision 10. In. Palisades, NY: NASA Socioeconomic Data and Applications Center (SEDAC)

Chen M, Wu S, Lei Y, Li S (2018) Study on embodied CO 2 transfer between the Jing-Jin-Ji region and other regions in China: a quantification using an interregional input-output model. Environ Sci Pollut Res 25:14068–14082

Cohen AJ, Brauer M, Burnett R, Anderson HR, Frostad J, Estep K, Balakrishnan K, Brunekreef B, Dandona L, Dandona R (2017) Estimates and 25-year trends of the global burden of disease attributable to ambient air pollution: an analysis of data from the Global Burden of Diseases Study 2015. Lancet 389:1907–1918

Gao Y, Feng Z, Li Y, Li S (2014) Freshwater ecosystem service footprint model: a model to evaluate regional freshwater sustainable development—a case study in Beijing–Tianjin–Hebei, China. Ecol Indic 39:1–9

Gelman A, Rubin DB (1992) Inference from iterative simulation using multiple sequences. Stat Sci 7:457–472

Heft-Neal S, Burney J, Bendavid E, Burke M (2018) Robust relationship between air quality and infant mortality in Africa. Nature 559:254–258

Huang T, Yu Y, Wei Y, Wang H, Huang W, Chen X (2018) Spatial–seasonal characteristics and critical impact factors of PM2. 5 concentration in the Beijing–Tianjin–Hebei urban agglomeration. PLoS One 13

Hystad P, Setton E, Cervantes A, Poplawski K, Deschenes S, Brauer M, Donkelaar AV, Lamsal L, Martin R, Jerrett M (2011) Creating national air pollution models for population exposure assessment in Canada. Environ Health Perspect 119:1123–1129

Kousa A, Kukkonen J, Karppinen A, Aarnio P, Koskentalo T (2002) A model for evaluating the population exposure to ambient air pollution in an urban area. Atmos Environ 36:2109–2119

Lelieveld J, Evans JS, Fnais M, Giannadaki D, Pozzer A (2015) The contribution of outdoor air pollution sources to premature mortality on a global scale. Nature 525:367–371

Li G, Haining R, Richardson S, Best N (2014) Space–time variability in burglary risk: a Bayesian spatio-temporal modelling approach. Spat Stat 9:180–191

Lunn DJ, Thomas A, Best N, Spiegelhalter D (2000) WinBUGS - a Bayesian modelling framework: concepts, structure, and extensibility. Stat Comput 10:325–337

Ni X, Cao C, Zhou Y, Cui X, Singh RP (2018) Spatio-temporal pattern estimation of PM2. 5 in Beijing-Tianjin-Hebei Region based on MODIS AOD and meteorological data using the back propagation neural network. Atmosphere 9:105

Peng J, Chen S, Lü H, Liu Y, Wu J (2016) Spatiotemporal patterns of remotely sensed PM2. 5 concentration in China from 1999 to 2011. Remote Sens Environ 174:109–121

Shen Y, Yao L (2017) PM2. 5, population exposure and economic effects in urban agglomerations of China using ground-based monitoring data. Int J Environ Res Public Health 14:716

van Donkelaar A, Martin RV, Brauer M, Boys BL (2015) Use of satellite observations for long-term exposure assessment of global concentrations of fine particulate matter. Environ Health Perspect 123:135–143

van Donkelaar A, Martin RV, Brauer M, Hsu NC, Kahn RA, Levy RC, Lyapustin A, Sayer AM, Winker DM (2016) Global estimates of fine particulate matter using a combined geophysical-statistical method with information from satellites, models, and monitors. Environ Sci Technol 50:3762–3772

Wang J-F, Hu Y (2012) Environmental health risk detection with GeogDetector. Environ Model Softw 33:114–115

Wang JF, Li XH, Christakos G, Liao YL, Zhang T, Gu X, Zheng XY (2010) Geographical detectors-based health risk assessment and its application in the neural tube defects study of the Heshun Region, China. Int J Geogr Inf Sci 24:107–127

Wang Y, Yao L, Wang L, Liu Z, Ji D, Tang G, Zhang J, Sun Y, Hu B, Xin J (2014) Mechanism for the formation of the January 2013 heavy haze pollution episode over central and eastern China. Sci China Earth Sci 57:14–25

Wang J-F, Zhang T-L, Fu B-J (2016) A measure of spatial stratified heterogeneity. Ecol Indic 67:250–256

Wang L, Xiong Q, Wu G, Gautam A, Jiang J, Liu S, Zhao W, Guan H (2019) Spatio-temporal variation characteristics of PM2. 5 in the Beijing–Tianjin–Hebei region, China, from 2013 to 2018. Int J Environ Res Public Health 16:4276

Yan D, Lei Y, Shi Y, Zhu Q, Li L, Zhang Z (2018) Evolution of the spatiotemporal pattern of PM2. 5 concentrations in China–a case study from the Beijing-Tianjin-Hebei region. Atmos Environ 183:225–233

Yang D, Wang X, Xu J, Xu C, Lu D, Ye C, Wang Z, Bai L (2018) Quantifying the influence of natural and socioeconomic factors and their interactive impact on PM2. 5 pollution in China. Environ Pollut 241:475–483

Zhao C, Wang Q, Ban J, Liu Z, Zhang Y, Ma R, Li S, Li T (2020) Estimating the daily PM2. 5 concentration in the Beijing-Tianjin-Hebei region using a random forest model with a 0.01°× 0.01° spatial resolution. Environ Int 134:105297

Zhong L, Louie PKK, Zheng J, Yuan Z, Yue D, Ho JWK, Lau AKH (2013) Science–policy interplay: air quality management in the Pearl River Delta region and Hong Kong. Atmos Environ 76:3–10